

# Thermoelectric Performance of Lead-Free Two-Dimensional Halide Perovskites Featuring Conjugated Ligands

Sheng-Ning Hsu, Wenchao Zhao, Yao Gao, Akriti, Mauricio Segovia, Xianfan Xu, Bryan W. Boudouris,\* and Letian Dou\*



Cite This: <https://doi.org/10.1021/acs.nanolett.1c02890>



Read Online

ACCESS |



Metrics & More



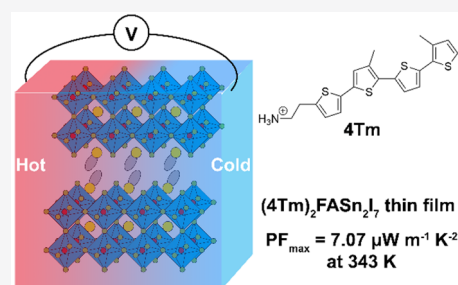
Article Recommendations



Supporting Information

**ABSTRACT:** Sn-based halide perovskites are promising for thermoelectric (TE) device applications because of their high electrical conductivity as well as the low thermal conductivity associated with their soft lattices. However, conventional three-dimensional Sn-based perovskites are not stable under typical TE device operating conditions. Here, we report a stable two-dimensional Sn-based perovskite for thermoelectric energy conversion by incorporating bulky conjugated ligands. We demonstrate a thin film with a large power factor of  $5.42 \pm 3.07$  (average) and  $7.07$  (champion)  $\mu\text{W m}^{-1} \text{K}^{-2}$  at 343 K with an electrical conductivity of  $5.07 \text{ S cm}^{-1}$  and a Seebeck coefficient of  $118.1 \mu\text{V K}^{-1}$ . Importantly, these thin films show excellent operational stability (i.e., for over 100 h) at 313 K. This work suggests that the novel hybrid two-dimensional perovskites are a promising platform for thermoelectric energy conversion applications.

**KEYWORDS:** Thermoelectric, Perovskites, Layers, Thin Films, Superlattices



Halide perovskites have received much interest in optoelectronic applications because of their promising light absorption and photoluminescence (PL) features, long carrier lifetime and diffusion length, and the fact that their nanostructures and optoelectronic properties can be tuned by controlling the composition of the materials. In addition, their solution-processability allows for low-cost, low-temperature, and large-area manufacturing.<sup>1,2</sup> Thus, many efforts have focused on generating high-performance perovskite-based photovoltaics (PVs),<sup>3</sup> light-emitting diodes,<sup>4</sup> and photodetectors.<sup>5</sup> In fact, current perovskite PVs have reached a maximum power conversion efficiency of 25.5%, and they are considered one of the most promising classes of semiconductors for emerging solar cell technologies.<sup>6</sup> Currently, commercialization of halide perovskite devices is hampered by the material's intrinsic instability under exposure to light and moisture, but two-dimensional (2D) halide perovskites are a possible replacement given their ability to overcome this critical limitation. By partially replacing the monovalent cations with relatively bulky organic ligands, halide perovskites are sliced into 2D layers sandwiched by the bulky ligands, and these ligands act as passivation layers that enhance the overall stability of the materials. Furthermore, the chemistry associated with the ligands opens new opportunities for tuning their end-use properties.<sup>7–11</sup> For instance, we recently demonstrated that by incorporation of bulky  $\pi$ -conjugated organic moieties, charge injection from the electrode to the perovskite layers can be improved and high-performance perovskite field-effect transistors were realized.<sup>12,13</sup> However,

this effort only scratched the surface of numerous applications of 2D perovskites that go well beyond solar energy conversion.

Thermoelectric (TE) devices are solid-state devices that interconvert electrical energy and thermal energy,<sup>14</sup> and due to their compact structure, TE devices are used in waste heat harvesting and cooling electronic components. The maximum efficiency of a TE device is limited by the dimensionless material figure-of-merit,  $ZT = (S^2\sigma/\kappa)T$ .<sup>15</sup> Here  $\sigma$ ,  $S$ ,  $\kappa$ , and  $T$  are the electrical conductivity, Seebeck coefficient, the thermal conductivity, and absolute temperature, respectively. Typically for semiconductors, the numerator of  $ZT$ , the power factor  $PF = S^2\sigma$ , can be modulated by several orders of magnitude by doping while the thermal transport properties are primarily controlled by the lattice thermal conductivity of the crystal. Recently, the thermoelectric performance of halide perovskites was theoretically predicted to be comparable with traditional bulk thermoelectric materials (e.g.,  $\text{Bi}_2\text{Te}_3$ ) due to their excellent Seebeck coefficients<sup>16,17</sup> and their “phonon glass, electron crystal” nature<sup>18</sup> (i.e., halide perovskites have both low  $\kappa$  and good charge carrier transport properties).<sup>19</sup> The low  $\kappa$  is the result of low sound velocities, dynamic disorder in their lattices, and strong acoustic phonon anharmonicity, which in

**Received:** July 27, 2021

**Revised:** August 26, 2021

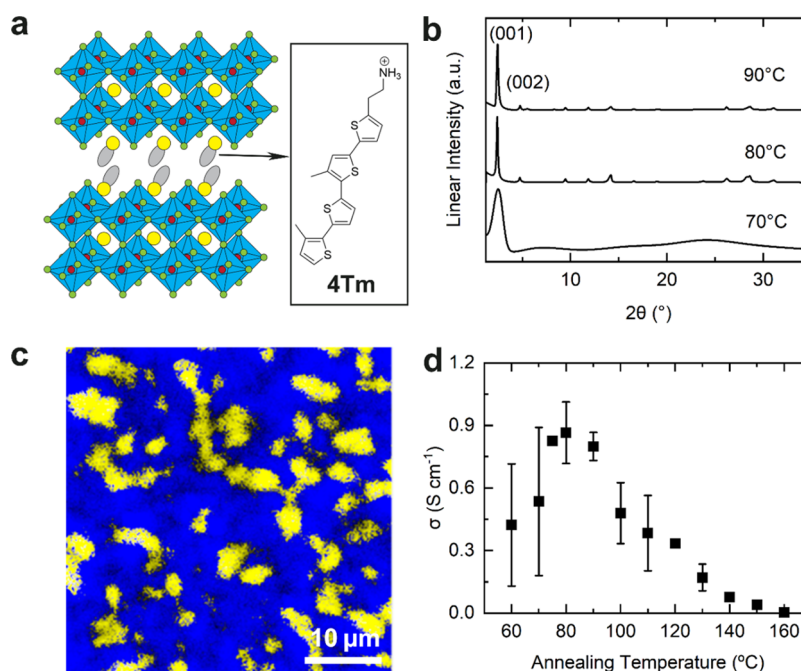


**Figure 1.** (a) Structure diagram of  $(4\text{Tm})_2\text{FASn}_2\text{I}_7$  thin film phase and the chemical structure of 4Tm. (b) XRD patterns of the thin films annealed at different temperatures. (c) Confocal PL of the thin film annealed at 80 °C. The color yellow corresponds to the  $n = 1$   $(4\text{Tm})_2\text{SnI}_4$  domains (597–695 nm), and the blue color corresponds to the  $n = 2$   $(4\text{Tm})_2\text{FASn}_2\text{I}_7$  (651–695 nm). (d) Room temperature electrical conductivity of the pristine (i.e., not doped) thin films with different annealing temperatures. The error bars indicate one standard deviation from the average value, which is indicated by the data points. These statistics were calculated across 26 thin films.

turn impedes phonon transport.<sup>20,21</sup> The reported  $\kappa$  of halide perovskites is around  $0.3\text{--}0.5\text{ W m}^{-1}\text{ K}^{-1}$ , a value approaching the amorphous limit.<sup>20,21</sup> Recently, a high ZT of 0.14 was achieved by Liu et al., demonstrating perovskites' great potential in thermoelectric energy harvesting applications.<sup>22–24</sup> However, halide perovskites, especially Sn-based perovskites, suffer from intrinsic instability and variation of doping levels when they are exposed to air. While the doping level is the most essential parameter to optimize the TE properties, engineering halide perovskites for higher stability is also of significant importance. 2D perovskites can aid in addressing both of these issues with their layered structure introduced by the hydrophobic bulky ligands that result in a quantum well structure.<sup>25–27</sup> Moreover, the hybrid organic–inorganic superlattice-like structure further reduces the thermal conductivity,<sup>28–31</sup> a principle that has long been established for traditional TE materials.<sup>32–34</sup> For instance, Wan et al. tripled the n-type ZT of  $\text{TiS}_2$  from  $\sim 0.08$  to 0.28 by intercalating hexylammonium into the  $\text{TiS}_2$  van der Waals gaps, forming an organic–inorganic hybrid superlattice. The ZT enhancement was primarily due to the lowered thermal conductivity, which was reduced from 4.45 to  $0.69\text{ W m}^{-1}\text{ K}^{-1}$ .<sup>33</sup> Similarly, the thermal conductivity of 2D perovskites was  $0.10\text{--}0.17\text{ W m}^{-1}\text{ K}^{-1}$ , less than one-third of their 3D counterparts.<sup>35</sup> These factors make 2D perovskites appealing as the next-generation solution-processable TE materials.

In this work, we demonstrate the potential of 2D perovskites in TE applications by synthesizing and characterizing a novel 2D perovskite  $(4\text{Tm})_2\text{FASn}_2\text{I}_7$  featuring a bulky ligand 2-(3''',4'-dimethyl[2,2':5'',2'':5''',2'''-quaterthiophen]-5-yl)ethan-1-ammonium (4Tm). In addition to its excellent hole transport capability, the hydrophobicity and bulkiness of the 4Tm ligand also provide materials stability, and the difference between its oxidative potential (i.e., +0.8 V vs Ag/AgCl) and the reductive

potential of  $\text{Sn}^{4+}$  (i.e.,  $-0.05$  vs Ag/AgCl) makes it highly compatible with the  $\text{Sn}^{4+}$  doping. That is, it is unlikely that the tin species will react with the conjugated ligand.<sup>7</sup> Using an artificial doping strategy (i.e., by doping with  $\text{Sn}^{4+}$ ), we were able to tune the carrier concentration of the p-type  $n = 2$   $(4\text{Tm})_2\text{FASn}_2\text{I}_7$  (Figure 1a) ranging from  $2 \times 10^{18}$  to  $1.2 \times 10^{19}\text{ cm}^{-3}$ , providing a robust way for the PF optimization. The champion device exhibited a high PF of  $7.07$  (average of  $5.42 \pm 3.07$ )  $\mu\text{W m}^{-1}\text{ K}^{-2}$  at 343 K. Furthermore, the substantially lower  $\kappa$  of  $0.124\text{ W m}^{-1}\text{ K}^{-1}$  compared with their 3D counterparts and excellent thermal stability highlight the potential of 2D perovskites as a class of low-cost, solution-processable TE materials.

The 2D perovskite thin films were fabricated using a facile solution-coating method. In this process, precursor solutions of  $(4\text{Tm})_2\text{FA}_2\text{Sn}_3\text{I}_{10}$  with a concentration of 0.05 M in  $N,N$ -dimethylformamide/dimethyl sulfoxide (11:1, v/v) were made and spun-coat onto the UV-ozone treated glass substrates inside a nitrogen-filled glovebox ( $\text{O}_2$ , <5 ppm;  $\text{H}_2\text{O}$ , <1 ppm). Followed by thermal annealing,  $\sim 90$  nm thick 2D perovskite films were formed. After the formation of 2D perovskite films, gold contacts were deposited in a van der Pauw configuration (Figure S1) for electrical conductivity, Hall effect, and Seebeck coefficient measurements. The XRD pattern (Figure 1b) of the resulting thin films has reflections at  $2\theta = 2.4^\circ$  and  $4.8^\circ$ , indicating that the interlayer distance is 36.8 Å, corresponding to the  $n = 2$   $(4\text{Tm})_2\text{FASn}_2\text{I}_7$ . Moreover, a small amount of the  $n = 1$   $(4\text{Tm})_2\text{SnI}_4$  phase exists according to the PL spectrum (Figure S2a), but they only form small clusters scattered within the large, continuous  $n = 2$  domains (Figure 1c). As such, we regard these thin films as  $n = 2$   $(4\text{Tm})_2\text{FASn}_2\text{I}_7$ .

Importantly, we found that annealing temperatures lower than 70 °C resulted in thin films showing wider and lower-intensity XRD reflections (Figure 1b and Figure S2b),

implying a lower degree of crystallinity. However, at annealing temperatures greater than 80 °C, we saw more discontinuities in the  $n = 2$  domains (Figure S3, images with wavelength of 651–695 nm), which may affect the overall charge transport. This was backed by the fact that the electrical conductivity is the highest when the annealing temperature is at 80 °C (Figure 1d). Given all these data, we implemented an annealing temperature of 80 °C for an annealing time of 5 min, which created the highest performing materials, in our hands.

Doping is a key handle by which to manipulate the thermoelectric performance of materials as an optimal doping level balances the trade-offs between TE parameters. In addition, establishing the relationship of TE parameters and the carrier concentration provides pathways to probe the band structure of the material. For the Sn-based halide perovskites, p-type doping usually results from Sn vacancies.<sup>36</sup> Moreover, the oxidation of Sn<sup>2+</sup> into Sn<sup>4+</sup> in the precursor solutions and the thin films can magnify the formation of Sn vacancies and thus amplify the p-doping effect.<sup>22,24,37</sup> As such, air exposure has been employed as an effective approach to control the doping level of Sn-based perovskites. However, our 2D perovskites exhibit much improved stability and the oxidation process is rather slow when they are exposed to air. Therefore, instead of exposing the samples to air, we introduced the Sn<sup>4+</sup> dopant by adding SnI<sub>4</sub> to the precursor solution to provide Sn<sup>4+</sup>. To control the doping level precisely, SnI<sub>2</sub>, 4TmI, formamidinium iodide (FAI), and the dilute SnI<sub>4</sub> solutions were used to make fresh solutions immediately before the thin films were cast. The detailed solution parameters are listed in Table S1. By intentionally doping the films, we controlled the carrier concentrations in a range between  $2 \times 10^{18}$  and  $1.2 \times 10^{19} \text{ cm}^{-3}$  (Figure S4). Moreover, the Hall effect measurement results indicate that the thin films are p-type as expected,<sup>22,24,38</sup> and the XRD patterns showed no noticeable change if the Sn<sup>4+</sup> content is lower than 1 mol % relative to Sn<sup>2+</sup> (Figure S5). Importantly, we note that the carrier concentration did not increase monotonically with SnI<sub>4</sub> content, most likely because extra Sn<sup>4+</sup> cations were expelled from the perovskite lattice.

We established the TE performance of 2D perovskites with varying carrier concentrations (Figure 2). The positive value of the Seebeck coefficient for the 2D perovskites agrees with the Hall effect measurement in that the majority carriers are holes, and there is a clear trade-off between  $\sigma$  and  $S$  due to the difference in doping level (Figure 2a and Figure 2b). This results in the PF reaching a maximum of  $2.44 \pm 0.48$  (average) and  $3.03$  (champion)  $\mu\text{W m}^{-1} \text{ K}^{-2}$  at an average absolute temperature of 293 K. The temperature-dependent TE parameters in the range of 263–353 K show that  $\sigma$  decreases and  $S$  increases as the temperature increases (Figure 3). The highest TE performance occurs when the carrier concentration reaches  $1.26 \times 10^{19} \text{ cm}^{-3}$ , which is the highest doping level we were able to attain. This implies that the TE performance could be higher if we were able to dope the thin films to a larger extent while maintaining the same crystal structure. The average PF reached a value of  $2.44 \pm 0.48 \mu\text{W m}^{-1} \text{ K}^{-2}$  at 293 K and  $5.49 \pm 3.07 \mu\text{W m}^{-1} \text{ K}^{-2}$  at 343 K. The champion sample showed a maximum PF of  $7.07 \mu\text{W m}^{-1} \text{ K}^{-2}$  at 343 K, which is the highest power factor for a 2D perovskite system reported to date. We also measured the thermal conductivity of the thin films using the differential  $3\omega$  method<sup>39</sup> and the time-domain thermoreflectance method (TDTR).<sup>40,41</sup> These data confirmed that 2D perovskites have much lower  $\kappa$  relative to their 3D counterparts with values of  $0.124 \text{ W m}^{-1} \text{ K}^{-1}$  (based

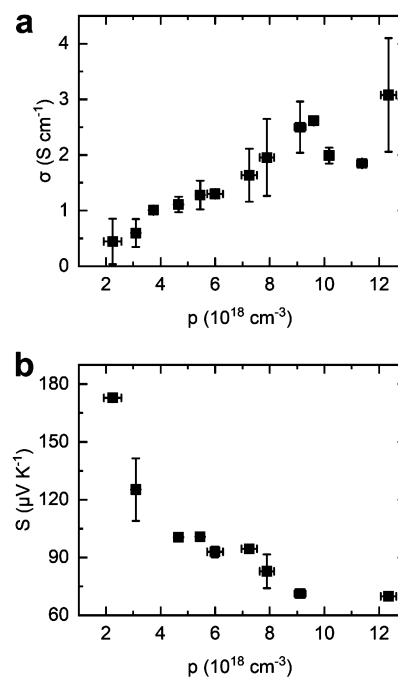


**Figure 2.** Dependence of the (a) electrical conductivity and (b) Seebeck coefficient on the carrier concentration of the 2D perovskite thin films at an average temperature of 293 K. Each data point shown is compiled from multiple data points whose carrier concentration values are approximately the same. The error bars in the horizontal directions indicate one standard deviation of carrier concentrations from the average value, and the error bars in the vertical direction indicate one standard deviation from the average value for either the electrical conductivity (a) or the Seebeck coefficient (b).

on the  $3\omega$  method) and  $0.146 \text{ W m}^{-1} \text{ K}^{-1}$  (based on the TDTR method) at room temperature (Figures S6 and S7). Combined with the PF of the thin films, the ZT of  $(4\text{Tm})_2\text{FASn}_2\text{I}_7$  is estimated to be  $\sim 0.02$  at room temperature. In addition to the doping level, the performance is mainly limited by the hole mobility ( $\mu$ ). Unlike previous efforts with 3D  $\text{CsSnI}_{3-x}\text{Cl}_x$  thin films, which have an average hole mobility of  $\sim 70 \text{ cm}^2 \text{ V}^{-1} \text{ s}^{-1}$ ,<sup>24</sup> the  $(4\text{Tm})_2\text{FASn}_2\text{I}_7$  has an average hole mobility at  $1.56 \text{ cm}^2 \text{ V}^{-1} \text{ s}^{-1}$ . One possible reason is the less-than-ideal morphology, as shown in the PL and optical microscopy images (Figure S8). Another plausible reason is the low phase purity of the film (coexistence of the  $n = 1$  and  $n = 2$  phases), which likely results in extra carrier scattering due to the band edge mismatch. Moreover, the organic ligands, which occupy approximately 83% of the total volume of the material, do not contribute as effective charge carrier channels. As such, these insights provide clear pathways for developing strategies to enhance the morphology, phase purity, and higher quantum well density as they are of great importance for 2D perovskites TE devices.

Excellent thermal stability is key for TE materials. To evaluate the thermal stability, we continuously monitored  $\sigma$  and  $S$  at 293, 313, and 333 K (Figure 4). The TE parameters were stable at 293 and 313 K for 100 h. The decrease in electrical conductivity at 313 K was due to a loss of contact between the instrument probes and the contact pads atop the perovskite thin film, and this was caused by the thermal cycling that necessarily occurred when acquiring data for the Seebeck coefficient evaluation. Thus, we occasionally adjusted the probes to reestablish good contacts, which resulted in the

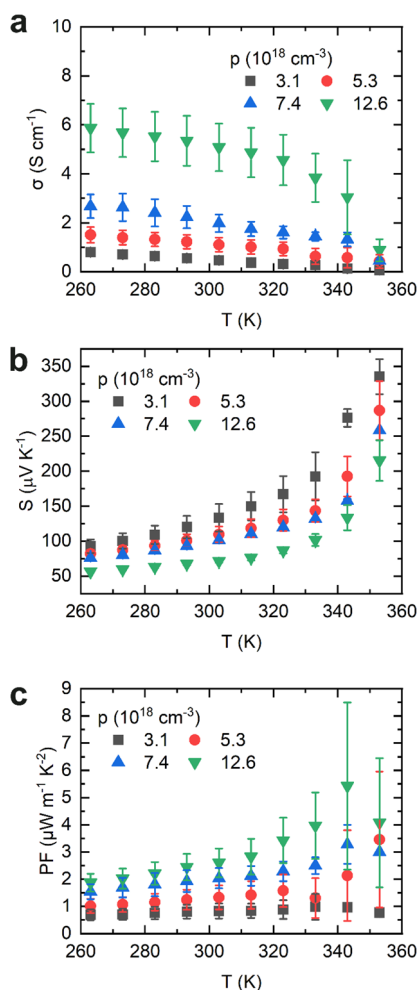


**Figure 3.** Dependence of the (a) electrical conductivity, (b) Seebeck coefficient, and (c) power factor on average temperatures of the 2D perovskite thin films. Each data point shown was compiled from multiple sets of data whose carrier concentration values are approximately the same, and different symbols represent the thermoelectric performance of different average carrier concentration values. The error bars indicate one standard deviation from the average value shown in the panels.

intermittent discontinuity of electrical conductivity. The results at 293 and 313 K indicate that the  $(4\text{Tm})_2\text{FASn}_2\text{I}_7$  thin films have good stability at these mild temperatures. Higher temperature (e.g., 333 K) causes the sample performances to decline mainly due to the drop in the electrical conductivity values. To investigate the changes caused by high temperature, a few samples were heated to an even higher temperature of 353 K for 3 h. The XRD traces and PL spectra of the thin films before and after the test show no noticeable change in phase (Figure S9). Instead, we observed an irreversible “dedoping” process, where the carrier concentration drops significantly after being heated to a higher temperature. Table 1 shows the carrier concentrations and mobility values of the thin films measured before and after the heating cycle. All perovskite films showed a decreased carrier concentration and constant mobility after operating at a high temperature, independent of the initial carrier concentration and mobility they had prior to the experiments. Therefore, we propose that the material underwent a thermal dedoping process where the lattice self-healed and excluded the  $\text{Sn}^{4+}$  ions and Sn vacant sites under

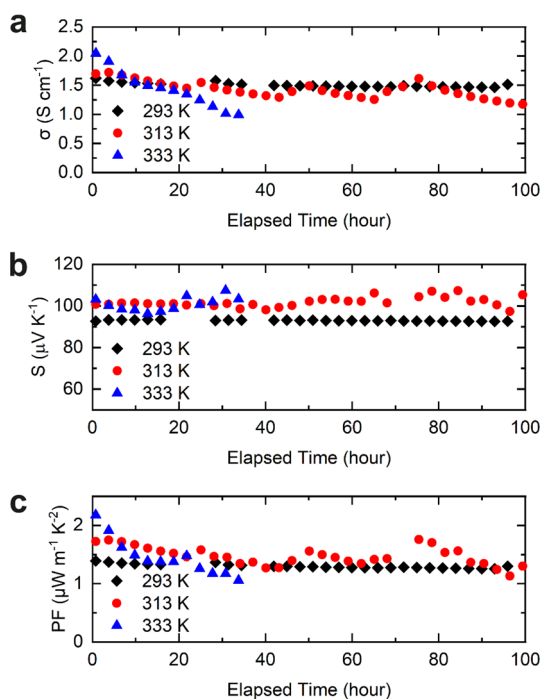


**Figure 4.** Thermal stability of the thin films at a fixed temperature: (a) electrical conductivity, (b) Seebeck coefficient, and (c) power factor versus elapsed time at 293, 313, and 333 K.

**Table 1.** Changes in the Carrier Concentrations and Mobility Values after Heating at 353 K for 3 h of Five Randomly Selected Samples<sup>a</sup>

no.	before measurement		after measurement	
	$\mu$ ( $\text{cm}^2 \text{V}^{-1} \text{s}^{-1}$ )	$p$ ( $\text{cm}^{-3}$ )	$\mu$ ( $\text{cm}^2 \text{V}^{-1} \text{s}^{-1}$ )	$p$ ( $\text{cm}^{-3}$ )
1	0.982	$2.96 \times 10^{18}$	0.729	$9.17 \times 10^{17}$
2	1.28	$3.34 \times 10^{18}$	0.913	$5.12 \times 10^{17}$
3	1.15	$5.27 \times 10^{18}$	1.15	$9.67 \times 10^{17}$
4	1.63	$5.49 \times 10^{18}$	1.58	$1.42 \times 10^{18}$
5	1.06	$1.21 \times 10^{19}$	1.19	$3.03 \times 10^{18}$

<sup>a</sup>All of the Hall effect measurements were conducted at 293 K.

higher temperature.<sup>42</sup> Additionally, the extremely low formation energy of the 4Tm-based perovskites and high defect tolerance make the defect exclusion feasible.<sup>12</sup> This result also explains, in part, why the higher annealing temperature results in lower electrical conductivity in Figure 1d.

In conclusion,  $(4\text{Tm})_2\text{FASn}_2\text{I}_7$  2D halide perovskite thin films are promising thermoelectric materials with a high PF of 3.03, 3.15, and  $7.07 \mu\text{W m}^{-1} \text{K}^{-2}$  at 293, 313, and 333 K, respectively. Furthermore, a clear dependency of electrical conductivity and Seebeck coefficient on carrier concentration and temperature is also established. Additionally, the thin films showed excellent thermal stability for more than 100 h when held at 293 and 313 K. Currently, the 2D perovskite performance is limited by the relatively low hole mobility compared with 3D Sn-based perovskites or other state-of-the-art thermoelectric materials; however, this work is a clear step forward for these nascent materials in this new application, and we envision that the thermoelectric performance of the Sn-based 2D perovskite materials will increase rapidly by employing the principles established here.

## ■ ASSOCIATED CONTENT

### SI Supporting Information

The Supporting Information is available free of charge at <https://pubs.acs.org/doi/10.1021/acs.nanolett.1c02890>.

Experimental details, PL light emission spectra, XRD patterns, confocal PL images, carrier concentration and mobility versus dopant concentration charts, optical microscopic images, PL images, AFM images, and thermal conductivity measurement data of the  $(4Tm)_2FASn_2I_7$  thin films (PDF)

## ■ AUTHOR INFORMATION

### Corresponding Authors

**Bryan W. Boudouris** – Charles D. Davidson School of Chemical Engineering and Department of Chemistry, Purdue University, West Lafayette, Indiana 47907, United States; [orcid.org/0000-0003-0428-631X](https://orcid.org/0000-0003-0428-631X); Email: [boudouris@purdue.edu](mailto:boudouris@purdue.edu)

**Lietian Dou** – Charles D. Davidson School of Chemical Engineering and Birck Nanotechnology Center, Purdue University, West Lafayette, Indiana 47907, United States; [orcid.org/0000-0001-6411-8591](https://orcid.org/0000-0001-6411-8591); Email: [dou10@purdue.edu](mailto:dou10@purdue.edu)

### Authors

**Sheng-Ning Hsu** – Charles D. Davidson School of Chemical Engineering, Purdue University, West Lafayette, Indiana 47907, United States; [orcid.org/0000-0001-7524-4251](https://orcid.org/0000-0001-7524-4251)

**Wenchao Zhao** – Charles D. Davidson School of Chemical Engineering, Purdue University, West Lafayette, Indiana 47907, United States

**Yao Gao** – Charles D. Davidson School of Chemical Engineering, Purdue University, West Lafayette, Indiana 47907, United States; [orcid.org/0000-0003-0172-8151](https://orcid.org/0000-0003-0172-8151)

**Akriti** – Charles D. Davidson School of Chemical Engineering, Purdue University, West Lafayette, Indiana 47907, United States; [orcid.org/0000-0002-8352-105X](https://orcid.org/0000-0002-8352-105X)

**Mauricio Segovia** – School of Mechanical Engineering and Birck Nanotechnology Center, Purdue University, West Lafayette, Indiana 47907, United States

**Xianfan Xu** – School of Mechanical Engineering and Birck Nanotechnology Center, Purdue University, West Lafayette, Indiana 47907, United States; [orcid.org/0000-0003-0580-4625](https://orcid.org/0000-0003-0580-4625)

Complete contact information is available at: <https://pubs.acs.org/10.1021/acs.nanolett.1c02890>

### Notes

The authors declare no competing financial interest.

## ■ ACKNOWLEDGMENTS

The work was supported the National Science Foundation (Award ECCS-1939986; Program Manager, Dr. Paul Lane). We thank Dr. Neil Dilley for helpful discussions and help with the Hall effect measurements and Wenlong Jin for help with the  $3\omega$  method.

## ■ REFERENCES

- (1) Manser, J. S.; Christians, J. A.; Kamat, P. V. Intriguing Optoelectronic Properties of Metal Halide Perovskites. *Chem. Rev.* **2016**, *116* (21), 12956–13008.
- (2) Shi, E.; Gao, Y.; Finkenauer, B. P.; Akriti; Coffey, A. H.; Dou, L. Two-dimensional halide perovskite nanomaterials and heterostructures. *Chem. Soc. Rev.* **2018**, *47* (16), 6046–6072.
- (3) Green, M. A.; Ho-Baillie, A. Perovskite Solar Cells: The Birth of a New Era in Photovoltaics. *ACS Energy Lett.* **2017**, *2* (4), 822–830.
- (4) Service, R. F. Perovskite LEDs begin to shine. *Science* **2019**, *364* (6444), 918.
- (5) Miao, J.; Zhang, F. Recent progress on highly sensitive perovskite photodetectors. *J. Mater. Chem. C* **2019**, *7* (7), 1741–1791.
- (6) National Renewable Energy Laboratory. Best research-cell efficiencies. <https://www.nrel.gov/pv/assets/pdfs/best-research-cell-efficiencies.20200925.pdf>.
- (7) Gao, Y.; Shi, E.; Deng, S.; Shiring, S. B.; Snaider, J. M.; Liang, C.; Yuan, B.; Song, R.; Janke, S. M.; Liebman-Pelaez, A.; Yoo, P.; Zeller, M.; Boudouris, B. W.; Liao, P.; Zhu, C.; Blum, V.; Yu, Y.; Savoie, B. M.; Huang, L.; Dou, L. Molecular engineering of organic-inorganic hybrid perovskites quantum wells. *Nat. Chem.* **2019**, *11* (12), 1151–1157.
- (8) Zimmermann, I.; Aghazada, S.; Nazeeruddin, M. K. Lead and HTM Free Stable Two-Dimensional Tin Perovskites with Suitable Band Gap for Solar Cell Applications. *Angew. Chem., Int. Ed.* **2019**, *58* (4), 1072–1076.
- (9) Maheshwari, S.; Savenije, T. J.; Renaud, N.; Grozema, F. C. Computational Design of Two-Dimensional Perovskites with Functional Organic Cations. *J. Phys. Chem. C* **2018**, *122* (30), 17118–17122.
- (10) Proppe, A. H.; Quintero-Bermudez, R.; Tan, H.; Voznyy, O.; Kelley, S. O.; Sargent, E. H. Synthetic Control over Quantum Well Width Distribution and Carrier Migration in Low-Dimensional Perovskite Photovoltaics. *J. Am. Chem. Soc.* **2018**, *140* (8), 2890–2896.
- (11) Passarelli, J. V.; Fairfield, D. J.; Sather, N. A.; Hendricks, M. P.; Sai, H.; Stern, C. L.; Stupp, S. I. Enhanced Out-of-Plane Conductivity and Photovoltaic Performance in  $n = 1$  Layered Perovskites through Organic Cation Design. *J. Am. Chem. Soc.* **2018**, *140* (23), 7313–7323.
- (12) Gao, Y.; Wei, Z.; Yoo, P.; Shi, E.; Zeller, M.; Zhu, C.; Liao, P.; Dou, L. Highly Stable Lead-Free Perovskite Field-Effect Transistors Incorporating Linear pi-Conjugated Organic Ligands. *J. Am. Chem. Soc.* **2019**, *141* (39), 15577–15585.
- (13) Gao, Y.; Wei, Z.; Hsu, S.-N.; Boudouris, B. W.; Dou, L. Two-dimensional halide perovskites featuring semiconducting organic building blocks. *Mater. Chem. Front.* **2020**, *4* (12), 3400–3418.
- (14) Bell, L. E. Cooling, heating, generating power, and recovering waste heat with thermoelectric systems. *Science* **2008**, *321* (5895), 1457–61.
- (15) Nolas, G. S.; Sharp, J.; Goldsmid, J. *Thermoelectrics: Basic Principles and New Materials Developments*; Springer Science & Business Media, 2013; Vol. 45.
- (16) He, Y.; Galli, G. Perovskites for Solar Thermoelectric Applications: A First Principle Study of  $CH_3NH_3Al_3(A = Pb \text{ and } Sn)$ . *Chem. Mater.* **2014**, *26* (18), 5394–5400.
- (17) Filippetti, A.; Caddeo, C.; Delugas, P.; Mattoni, A. Appealing Perspectives of Hybrid Lead–Iodide Perovskites as Thermoelectric Materials. *J. Phys. Chem. C* **2016**, *120* (50), 28472–28479.
- (18) Miyata, K.; Atallah, T. L.; Zhu, X. Y. Lead halide perovskites: Crystal-liquid duality, phonon glass electron crystals, and large polaron formation. *Sci. Adv.* **2017**, *3* (10), e1701469.
- (19) Beekman, M.; Morelli, D. T.; Nolas, G. S. Better thermoelectrics through glass-like crystals. *Nat. Mater.* **2015**, *14* (12), 1182–5.
- (20) Xie, H.; Hao, S.; Bao, J.; Slade, T. J.; Snyder, G. J.; Wolverton, C.; Kanatzidis, M. G. All-Inorganic Halide Perovskites as Potential Thermoelectric Materials: Dynamic Cation off-Centering Induces Ultralow Thermal Conductivity. *J. Am. Chem. Soc.* **2020**, *142* (20), 9553–9563.
- (21) Haque, M. A.; Kee, S.; Villalva, D. R.; Ong, W. L.; Baran, D. Halide Perovskites: Thermal Transport and Prospects for Thermoelectricity. *Adv. Sci.* **2020**, *7* (10), 1903389.

- (22) Takahashi, Y.; Hasegawa, H.; Takahashi, Y.; Inabe, T. Hall mobility in tin iodide perovskite  $\text{CH}_3\text{NH}_3\text{SnI}_3$ : Evidence for a doped semiconductor. *J. Solid State Chem.* **2013**, *205*, 39–43.
- (23) Haque, M. A.; Nugraha, M. I.; Paleti, S. H. K.; Baran, D. Role of Compositional Tuning on Thermoelectric Parameters of Hybrid Halide Perovskites. *J. Phys. Chem. C* **2019**, *123* (24), 14928–14933.
- (24) Liu, T.; Zhao, X.; Li, J.; Liu, Z.; Liscio, F.; Milita, S.; Schroeder, B. C.; Fenwick, O. Enhanced control of self-doping in halide perovskites for improved thermoelectric performance. *Nat. Commun.* **2019**, *10* (1), 5750.
- (25) Dou, L. Emerging two-dimensional halide perovskite nanomaterials. *J. Mater. Chem. C* **2017**, *5* (43), 11165–11173.
- (26) Dou, L.; Wong, A. B.; Yu, Y.; Lai, M.; Kornienko, N.; Eaton, S. W.; Fu, A.; Bischak, C. G.; Ma, J.; Ding, T.; Ginsberg, N. S.; Wang, L. W.; Alivisatos, A. P.; Yang, P. Atomically thin two-dimensional organic-inorganic hybrid perovskites. *Science* **2015**, *349* (6255), 1518–21.
- (27) Quan, L. N.; Yuan, M.; Comin, R.; Voznyy, O.; Beaugregard, E. M.; Hoogland, S.; Buin, A.; Kirmani, A. R.; Zhao, K.; Amassian, A.; Kim, D. H.; Sargent, E. H. Ligand-Stabilized Reduced-Dimensionality Perovskites. *J. Am. Chem. Soc.* **2016**, *138* (8), 2649–55.
- (28) Kim, R.; Datta, S.; Lundstrom, M. S. Influence of dimensionality on thermoelectric device performance. *J. Appl. Phys.* **2009**, *105* (3), 034506.
- (29) Balandin, A. A.; Nika, D. L. Phononics in low-dimensional materials. *Mater. Today* **2012**, *15* (6), 266–275.
- (30) Kothari, K.; Maldovan, M. Phonon Surface Scattering and Thermal Energy Distribution in Superlattices. *Sci. Rep.* **2017**, *7* (1), 5625.
- (31) Hicks, L. D.; Dresselhaus, M. S. Effect of quantum-well structures on the thermoelectric figure of merit. *Phys. Rev. B: Condens. Matter Mater. Phys.* **1993**, *47* (19), 12727–12731.
- (32) Caylor, J. C.; Coonley, K.; Stuart, J.; Colpitts, T.; Venkatasubramanian, R. Enhanced thermoelectric performance in PbTe-based superlattice structures from reduction of lattice thermal conductivity. *Appl. Phys. Lett.* **2005**, *87* (2), 023105.
- (33) Wan, C.; Gu, X.; Dang, F.; Itoh, T.; Wang, Y.; Sasaki, H.; Kondo, M.; Koga, K.; Yabuki, K.; Snyder, G. J.; Yang, R.; Koumoto, K. Flexible n-type thermoelectric materials by organic intercalation of layered transition metal dichalcogenide  $\text{TiS}_2$ . *Nat. Mater.* **2015**, *14* (6), 622–7.
- (34) Dresselhaus, M. S.; Chen, G.; Tang, M. Y.; Yang, R. G.; Lee, H.; Wang, D. Z.; Ren, Z. F.; Fleurial, J. P.; Gogna, P. New Directions for Low-Dimensional Thermoelectric Materials. *Adv. Mater.* **2007**, *19* (8), 1043–1053.
- (35) Giri, A.; Chen, A. Z.; Mattoni, A.; Aryana, K.; Zhang, D.; Hu, X.; Lee, S. H.; Choi, J. J.; Hopkins, P. E. Ultralow Thermal Conductivity of Two-Dimensional Metal Halide Perovskites. *Nano Lett.* **2020**, *20* (5), 3331–3337.
- (36) Euvrard, J.; Yan, Y. F.; Mitzi, D. B. Electrical doping in halide perovskites. *Nat. Rev. Mater.* **2021**, *6* (6), 531–549.
- (37) Ricciarelli, D.; Meggiolaro, D.; Ambrosio, F.; De Angelis, F. Instability of Tin Iodide Perovskites: Bulk p-Doping versus Surface Tin Oxidation. *ACS Energy Lett.* **2020**, *5* (9), 2787–2795.
- (38) Takahashi, Y.; Obara, R.; Lin, Z. Z.; Takahashi, Y.; Naito, T.; Inabe, T.; Ishibashi, S.; Terakura, K. Charge-transport in tin-iodide perovskite  $\text{CH}_3\text{NH}_3\text{SnI}_3$ : origin of high conductivity. *Dalton Trans.* **2011**, *40* (20), 5563–8.
- (39) Cahill, D. G.; Katiyar, M.; Abelson, J. R. Thermal conductivity of a-Si:H thin films. *Phys. Rev. B: Condens. Matter Mater. Phys.* **1994**, *50* (9), 6077–6081.
- (40) Cahill, D. G. Analysis of heat flow in layered structures for time-domain thermoreflectance. *Rev. Sci. Instrum.* **2004**, *75* (12), 5119–5122.
- (41) Schmidt, A. J.; Chen, X.; Chen, G. Pulse accumulation, radial heat conduction, and anisotropic thermal conductivity in pump-probe transient thermoreflectance. *Rev. Sci. Instrum.* **2008**, *79* (11), 114902.
- (42) Ran, C.; Gao, W.; Li, J.; Xi, J.; Li, L.; Dai, J.; Yang, Y.; Gao, X.; Dong, H.; Jiao, B.; Spanopoulos, I.; Malliakas, C. D.; Hou, X.; Kanatzidis, M. G.; Wu, Z. Conjugated Organic Cations Enable Efficient Self-Healing  $\text{FASnI}_3$  Solar Cells. *Joule* **2019**, *3* (12), 3072–3087.